

**Department of Physics and Astronomy  
Heidelberg University**

Bachelor Thesis in Physics  
submitted by Alberto Rodríguez Concepción

# **Alberto Rodríguez Concepción**

born in Las Palmas de Gran Canaria (Spain)

**2021**

# **Construction of a Heidelberg Compact electron beam ion trap for high resolution measurements with the novel metallic magnetic calorimeter maXs-30**

This Bachelor Thesis has been carried out by Alberto Rodríguez Concepción at the  
Max Planck Institute for Nuclear Physics in Heidelberg  
under the supervision of  
apl. Prof. Dr. José R. Crespo López-Urrutia



## **Abstract**

In this work a new Heidelberg Compact electron beam ion trap (HC-EBIT) has been built, with the intention to be used in conjunction with a maXs-30, a low temperature metallic magnetic calorimeter. EBITs in the HC-EBIT series are capable of beam currents of up to 80 mA and energies up to 10 keV. The constructed HC-EBIT produces a magnetic of 860 mT at the trap centre, in accordance with the other EBITs in the series. In the first tests the EBIT produced beam currents of up to 6 mA while maintaining transmissions above 95% before malfunctioning. While the EBIT was operational a proof-of-principle experiment was designed, where the spectra of argon gas injected into the interaction zone was recorded with a Silicon Drift Detector. At the time of writing of this thesis a problem in the drift-tube assembly has been hypothesised as a cause of the malfunction that will hopefully be resolved soon. The objective of this work is to explain and document the building process of the EBIT, while providing the theoretical background relevant to its understanding.

## **Zusammenfassung**

In dieser Arbeit wurde eine neue Heidelberg Compact Elektronenstrahl-Ionenfalle (HC-EBIT) gebaut, die in Verbindung mit einer maXs-30-Maschine, einem Metallisch magnetischer Kalorimeter, verwendet werden soll. EBITs der HC-EBIT Serie sind in der Lage, Strahlströme von bis zu 80 mA, Energien von bis zu 10 keV zu erzeugen. Die konstruierte HC-EBIT erzeugt ein Magnetfeld von 860 mT im Fallenzentrum, wie die anderen EBITs der Serie. Bei den ersten Tests produzierte die EBIT, Strahlströme von bis zu 6 mA, während sie Transmissionen in den Bereichen von über 95% aufrechterhielt bevor sie ausfiel. Während die EBIT in Betrieb war, wurde ein Proof-of-Concept-Experiment entworfen, bei dem die Spektren von Argongas, das in die Wechselwirkungszone injiziert wurde, mit einem Silizium-Drift-Detektor aufgezeichnet wurden. Zum Zeitpunkt der Abfassung dieser Arbeit wurde ein Problem in der Driftröhre als Ursache für die Fehlfunktion vermutet was hoffentlich bald behoben wird. Ziel dieser Arbeit ist es, den Bauprozess der EBIT zu erläutern und zu dokumentieren und gleichzeitig den theoretischen Hintergrund zu vermitteln, der für das Verständnis der EBIT relevant ist.



# Contents

<b>1</b>	<b>Introduction</b>	<b>9</b>
<b>2</b>	<b>Theoretical background</b>	<b>11</b>
2.1	The atom . . . . .	11
2.2	Highly charged ions . . . . .	14
2.3	Interactions inside the EBIT . . . . .	14
2.3.1	Ionization . . . . .	14
2.3.2	Excitation . . . . .	15
2.3.3	Recombination . . . . .	15
2.3.4	De-excitation . . . . .	16
2.3.5	Overview of the building blocks . . . . .	16
2.4	The EBIT . . . . .	18
2.4.1	The electron beam . . . . .	19
2.5	Microcalorimeters . . . . .	20
<b>3</b>	<b>Building process</b>	<b>21</b>
3.1	Overall structure . . . . .	21
3.1.1	The common elements . . . . .	21
3.1.2	The unique setup . . . . .	22
3.2	The magnetic structure . . . . .	26
3.2.1	Assembling the magnetic structure . . . . .	26
3.2.2	Measuring the magnetic structure . . . . .	26
3.3	The electron gun . . . . .	28
3.4	The drift tubes . . . . .	31
3.5	The collector . . . . .	34
3.6	The vacuum system . . . . .	36
3.7	Injection system . . . . .	40
<b>4</b>	<b>A first spectrum</b>	<b>43</b>
4.1	Calibration . . . . .	43
4.2	The argon spectrum . . . . .	46
<b>5</b>	<b>Summary and outlook</b>	<b>49</b>





# 1 Introduction

Highly charged ions (HCIs), understood as ions with a majority of its electrons being removed, are a seldom encounter in this planet. Nevertheless, most of the matter in the visible universe is made out of HCIs [4]. HCIs, found ubiquitous in hot plasma, typically leave an X-ray trace behind, difficult to observe from beneath our protective atmosphere. One of the efforts to augment the vision of the universe was Hitomi, (Japanese for pupil). Hitomi, which launched in 2016, was a satellite, equipped with a microcalorimeter among other instrument, intended for high resolution X-ray astronomy. It was planned for Hitomi to provide data for about 3 years, unfortunately after a series of problems with attitude control, after only a bit over a month of service Hitomi began spinning uncontrollably leading to its subsequent breakage [2].

Gladly other space observatories like XMM-Newton and Chandra, which are equipped with high resolution spectrometers, had and continue to provide a longer service time of over 20 years. XMM-Newton was launched in 1999 and is capable of imaging in optical and X-ray wavelength [1] and Chandra launched in the same year [11], observed signals produced by HCIs ever since they first launched.

X-ray satellites have not fallen out of favor. They remain as relevant as ever, as evidenced by many other X-ray satellites and the imminent launch of XRISM [7].

The study of highly charged ions alone does not require the launch of satellites into space. Devices like electron beam ion traps (EBITs) prove to be a reliable source for the production of HCIs. In the past decades, it has been shown that the spectroscopy of highly charged ions in the laboratory can be used for testing and providing inside into the atomic structure as well as astrophysical models that assist the analysis of astrophysical spectra. Applications of HCIs are not only found in the field of physics and astrophysics. HCIs already find applications in fields as varied as medicine, in the treatment of cancer [6], or in ion lithography, used in the production of microchips [12]. Another area where HCIs could prove to be useful is quantum computing [6], an area that could revolutionize the use of technology.

For all this reasons it is crucial to study and understand HCIs by the means of spectroscopy. State of the art microcalorimeters can assist in deepening the understanding. The low temperature metallic magnetic calorimeters maXs-30 developed in the group of Gastaldo at the Kirchhoff Institute for Physics allows high resolution measurements with average resolution of 6.1 eV FWHM [17], an improvement of an order of magnitude compared to modern silicon based detectors. In this work a new Heidelberg Compact EBIT is designed and build to allow a symbiotic operation between the EBIT and the

calorimeter with the goal to obtain high resolution spectra of highly charged ions.

This thesis will document the building process of the constructed HC-EBIT. In the following chapters an overview of the theoretical background needed to understand the atomic structure, HCIs and the processes that occur inside an EBIT is given. A brief explanation of EBITs and Metallic Magnetic Calorimeters will follow. The building process and some of the design decisions will be described while explaining highlighted parts. Finally a proof-of-principle experiment will be presented.

## 2 Theoretical background

### 2.1 The atom

Niels Bohr described a model where the electrons revolve around the nucleus in discrete orbits [14]. In his depiction, the bound electrons lose or gain energy by absorbing or emitting electromagnetic radiation when jumping between orbits.

Bohr concluded that the angular momentum of the electrons  $L$  had to be a quantised quantity:

$$L = n\hbar \quad (2.1)$$

where  $\hbar$  is the reduced Planck constant with a value of  $1.054\,571\,817 \dots \times 10^{-34}$  J s [16] and  $n$  can only be an integer, called the *principal quantum number*. This quantization implies that orbit radius and energy have to be quantized too.

This orbit is referred to as *energy level*.

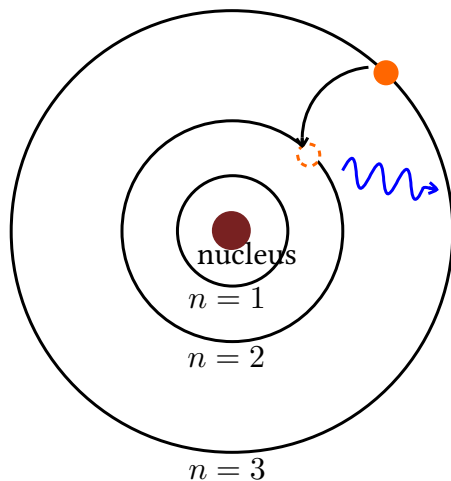


Figure 2.1: An electron emitting electromagnetic radiation as depicted in the Bohr model. The electron (orange) emits a photon (blue) while jumping from the third orbital into the second orbital.

The call to fame of the Bohr model was its ability to explain formula 2.2, the Rydberg formula, a formula that had been found empirically[13]:

$$\frac{1}{\lambda} = R_H \left( \frac{1}{n_1^2} - \frac{1}{n_2^2} \right) \quad (2.2)$$

It predicts the wavelength  $\lambda$  of the spectral lines that result from electrons jumping between two orbitals  $n_1$  and  $n_2$ .  $R_H$  is the so called *Rydberg constant for Hydrogen*. Expressed in terms of the energy-levels and extended for any Hydrogen-like element of atomic number  $Z$  the formula becomes:

$$E_n = E_R \cdot \frac{Z^2}{n^2} \quad , \quad (2.3)$$

where  $E_R$  is the *Rydberg-Energy*.

This formulas can already describe the energy levels of the Hydrogen atom or Hydrogen-like atoms (that is atoms with one electron) to a very high accuracy.

Since Bohr presented his model in 1913 there have been many refinements made to it, like the Bohr-Sommerfeld model. However it was not until the introduction of the Schrödinger equation that a significant breakthrough led to a more in depth understanding of the atomic structure.

Now considered one of the most fundamental equations governing the quantum world, the Schroedinger equation provides a formalism that utilizes so called *wave functions*. These wave functions describe the probability of finding a particle in specific space region.

$$i\hbar \frac{\partial}{\partial t} |\psi(t)\rangle = \hat{H} |\psi(t)\rangle \quad (2.4)$$

Where  $\psi$  is the state vector,  $t$  is the time and  $\hat{H}$  the Hamiltonian operator.

The Schroedinger equation can only be solved analytically for a small amount of problems. It is therefore imperative to understand those problems extensively.

In the following an outline of how to do so for Hydrogen like-particles is given:

The *central potential* given by an Atom of atomic mass  $Z$  in spherical coordinates is

$$V(r) = \frac{-Ze^2}{r} \quad , \quad (2.5)$$

where  $r$  is the radial distance from the coordinate. So the Hamiltonian of the problem becomes:

$$\hat{H} = -\frac{\hbar^2}{2m} \nabla_r^2 + V(r) = -\frac{\hbar^2}{2m} \nabla_r^2 - \frac{Ze^2}{r} \quad , \quad (2.6)$$

where  $\nabla_r^2$  indicates the *Laplacian in spherical coordinates*

One can assume that the wave function that solves the problem constitutes of two independent functions, with this approach one can find the solution to the problem, which is:

$$\psi(r, \theta, \phi) = R(r)_{nl} Y_{lm}(\theta, \phi) \quad (2.7)$$

Where  $R(r)_{nl}$  is the radial wave function and  $Y_{lm}(\theta, \phi)$  the spherical harmonics. The indices  $l$  and  $m$  indicate the angular momentum- and the magnetic quantum number respectively.

The Schrödinger equation does not portray the full picture. Refinements to the Schrödinger equation take into account *spin interactions* and *relativistic effects*. This two refinements account for a shift in the energy levels called *fine structure*.

Another refinement responsible for the so called *super fine structure* is the *lamb shift*, which takes into account interactions due to vacuum energy fluctuations.

## 2.2 Highly charged ions

When a bound electron is removed from an atom, an ion is produced. By removing enough bound electrons a highly charged ion (HCI) is produced. The vagueness that the term “enough bound electrons” denotes is intentional, since the distinction between ion and highly charged ion is not a clear one.

Some people talk about a majority of electrons having to be removed, while for others the numbers of electrons that have to be removed may be higher or lower than that.

When referring to an atom  $X$  one can write its charged state as  $X^q$ . The charge state is  $q$  or  $q+$ , written in Arabic numerals, such that  $Fe^{13+}$  is iron with 13 missing electrons. Spectroscopic notation represents the charge state of an atom with roman numeral to the right of its chemical symbol but considers an element with the numeral I to be the neutral of its kind. This way  $Fe^{0+}$  as well as  $FeI$  are the neutral element iron and  $Fe^{13+}$  as well as  $FeXIV$  are iron with 13 missing electrons.

Another way of describing the number of remaining electrons in an ion is by referring to them as being the alike to the neutral atom that has the same number of electrons. Electrons with one, two or three remaining electrons are referred to as hydrogen-, helium- or lithium-like atoms respectively. When talking about an atom that has had all its electrons removed, the term fully ionized atom is used.

## 2.3 Interactions inside the EBIT

### 2.3.1 Ionization

#### Electron impact ionization EII

The process that allows HCIs to be produced inside an EBIT is called *electron impact ionization*. When an electron with sufficient energy hits an atom, the impacting electron could transfer enough energy to detach an atoms electron from its orbital.

In this process, an ion  $X$  with charge  $q$ , gets hit by an electron  $e^-$ :



For this process to occur, the energy of the incoming electron  $E_{in}$  has to be greater than the binding-energy  $E_B$  of the atom. Such that:

$$E_{in} = E_B + E_1 + E_2 \quad (2.9)$$

Where  $E_1$  is the energy of one of the outcoming electrons and  $E_2$  is the energy of the second outcoming electron.

## Photoionization

A photon  $\gamma$  can also ionize an atom in a process called *photoionization*:



The energy of the photon  $E_\gamma$  has to be greater than the binding energy of the electron  $E_B$  for this process to be possible. Any excess of the ionized state is transferred to the outgoing electron in the form of kinetic energy:

$$E_\gamma = E_B + E_{kin} \quad (2.11)$$

## 2.3.2 Excitation

### Electron impact excitation (EIE)

An incident electron could also interact with an atom, transferring enough energy to excite the atom without ionizing it or being captured by it, in a process called *electron impact excitation*:



Here  $X^*$  denotes the atom in an excited state. The kinetic energy of the electron will be decreased by the amount of energy the atom gained.

### Photon excitation

An Atom can also get into an excited state when absorbing a photon. This process is called *photon excitation*.



It is of importance to point out, that while an electron can transfer part of its energy to another electron, a photon can only be absorbed by an atom resonantly, that is to say, the energy has to match the energy difference between two energy levels  $E_n$  and  $E_{n'}$ .

$$E_\gamma = E_n - E_{n'} \quad (2.14)$$

## 2.3.3 Recombination

### Electronic recombination

An atom can recombine with an electron, leaving the atom in an excited state. Atoms in excited states are generally short lived and will de-excite like explained later in the text.



## Radiative recombination (RR)

*Radiative recombination* is the process in which an atom captures an incident electron emitting a photon:



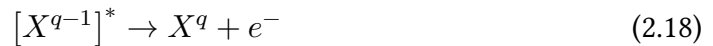
The photon energy has to be equal to the kinetic energy of the incoming electron plus the released binding energy.

$$E_\gamma = E_{kin} + E_B \quad (2.17)$$

### 2.3.4 De-excitation

#### Auger decay

*Auger decay*, also known as *autoionization* is the process where an excited atom radiates an electron, lowering its charged state:



#### Radiative decay

An excited atom can also de-excite by *radiative decay*, maintaining its charged state:



The energy difference between the excited atom and its non-excited counterpart is emitted in the form of a photon.

### 2.3.5 Overview of the building blocks

The aforementioned interactions can be seen as the building blocks of all the interactions that occur inside of an EBIT, since they represent the most fundamental interactions between a particle and an atom. Atoms can be ionized by an interaction with either a photon or an electron and they can recombine with an electron, leaving an excited atom or emitting a photon.

Atoms can be excited without a change in its charge state by an electron or a photon and can be de-excited by emitting an electron, in which case its charged state is altered, or by emitting a photon.

Of course these are not the only interactions possible, e.g. interactions involving multiple particles have been left out.



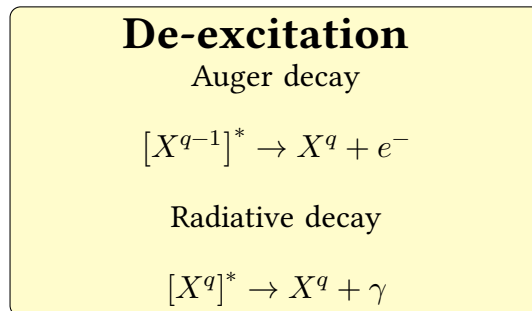
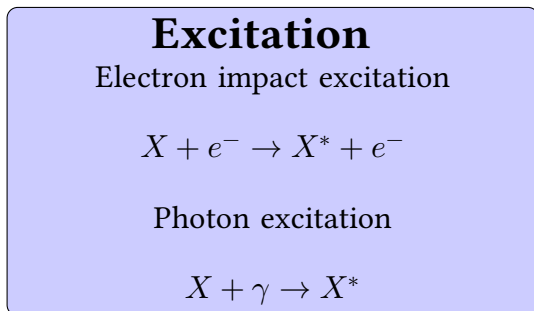
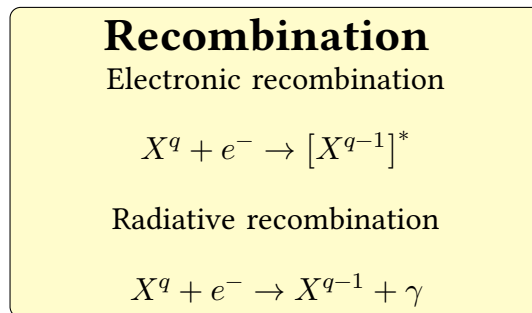
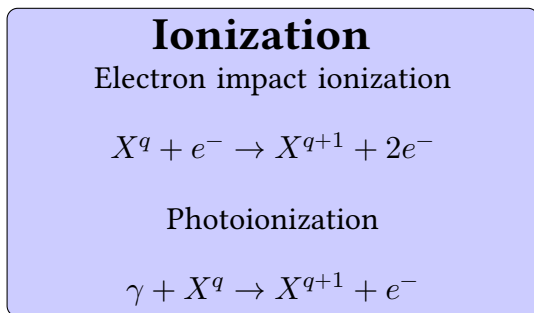


Figure 2.2: Overview of the fundamental processes inside an EBIT.

## 2.4 The EBIT

An electron beam ion trap (EBIT), as the acronym hints to, is a machine capable of generating an electron beam suitable for the production of and trapping of ions. Invented by *M. Levine and R. Marrs* and first presented in 1988 [9] they can be viewed as the successor of a different machine, the so called electron beam ion source (EBIS). EBIS are based upon the serendipitous found fundamental principle that an electron beam would trap ions by its own space charge. The basic working principle of an EBIT is represented in figure 2.3. An electron gun produces an electron beam that is guided and accelerated towards the collector by the drift tubes. The electron beam then interacts with the atoms injected at the trap center, ionizing them by electron impact ionization. Since the electrons forming the electron beam repel each other, the beam has to be compressed by a magnetic field. A compact electron density at the trap center enhances the electron impact ionization process described in the previous section. The ions are then trapped radially by the negative space charge of the electron beam itself, as well as the Lorentzian motion imposed upon them by the magnetic field. Axially the ions are trapped by the potential well shaped by a drift tube setup.

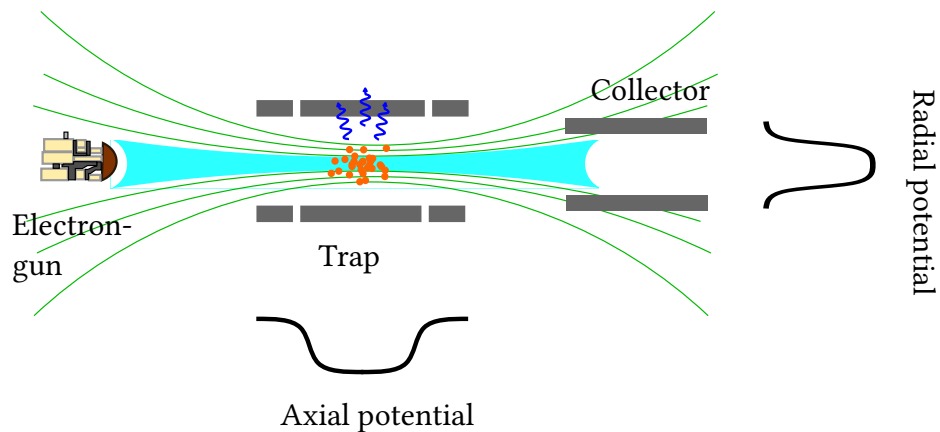


Figure 2.3: A schematic representation of the fundamental concept of an EBIT. The (light blue) electron beam gets compressed by the magnetic field (the magnetic field lines are depicted in green). The ions in the ion cloud (orange), trapped by the axial and radial potential get ionized and emit electromagnetic radiation (blue). The beam is dumped at the collector.

## 2.4.1 The electron beam

The following parameters characterise the electron beam at the trap center.

### Radius

The Hermann radius  $r_H$  [8] describes the radius that contains 80% of the electrons in the beam:

$$r_H = \sqrt{\frac{m_e I}{\pi \epsilon_0 e v B^2} + \sqrt{\left(\frac{m_e I}{\pi \epsilon_0 e v B^2}\right)^2 + \frac{8 k_B T_c m_e}{e^2 B^2} r_c^2 + \frac{B_c^2}{B^2} r_c^4}} \quad . \quad (2.20)$$

In the formula  $I$  is the electron beam current  $v$  the velocity of the electrons,  $B$  the magnetic field strength at the trap center,  $k_B$  the Boltzmann constant and  $r_c$ ,  $B_c$ ,  $T_c$  the radius of-, the magnetic field at- and the temperature of- the cathode respectively.

This radius can be used to calculate the charge density

$$\rho = \frac{I}{\pi r_H^2 v} \quad . \quad (2.21)$$

### Energy

The beam energy in the trap centre is approximated by the potential difference between the cathode and the central drift tube. In addition to that the energy has to be corrected to account for the potential caused by the attraction of the ions and the repulsion of the electrons.

$$E_{Beam} = e (-\phi_{cathode} + \phi_{trap} + \phi_{ions} - \phi_{electrons}) \quad . \quad (2.22)$$

The simpler estimation

$$E_{beam} = (U_{trap} - U_{cathode}) \quad , \quad (2.23)$$

where  $U_{trap}$  denotes the voltage applied to the central drift tube and  $U_{cathode}$  the one applied to the cathode turns out to be a very good approximation.

It is important to note that in the EBIT  $U_{cathode}$  is negative.

## 2.5 Microcalorimeters

Calorimetry is the measurement of heat transfer in or out of a system.

Metallic magnetic calorimeters (MMCs) are particle detectors that rely upon calorimetry principles to resolve energies with very high accuracy. They are therefore well suited for high resolution X-ray spectroscopy.

A metallic magnetic calorimeter uses a metallic absorber and a paramagnetic sensor to detect the magnetization of the paramagnetic sensor. This magnetization changes are related to the absorbed energy [5].

The metallic absorber absorbs the incident radiation. The thereby deposited energy causes a small temperature increase in the metallic absorber and paramagnetic sensor. Since the magnetization of the paramagnetic sensor is temperature dependent, the change in temperature leads to a change of the magnetization. The change in magnetization is in turn proportional to the magnetic flux. Magnetic flux differences can be detected by a superconducting coil and converted into voltages that are proportional to the energy of the incident particle. A weak thermal coupling between the paramagnetic sensor and a thermal bath will ensure that the sensor and absorber return to their original temperature.

# 3 Building process

## 3.1 Overall structure

### 3.1.1 The common elements

The EBIT build in the framework of this work is part of a series of similar EBITs that fall under the name of Heidelberg Compact electron beam ion trap (HC-EBIT) [10]. While they all serve different purposes, they share the core components shown in figure 3.1.

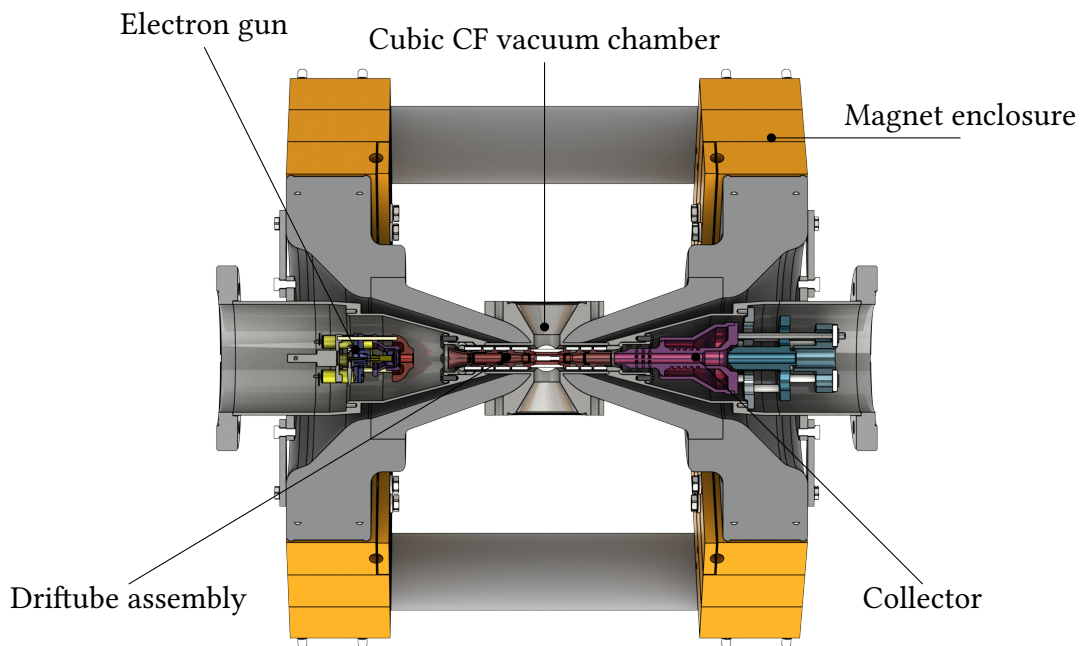


Figure 3.1: A rendered cross section of the CAD model of the HC-EBIT where the most important components shared by all HC-EBITs are visible.

A central cubic CF vacuum chamber houses the drift tube assembly that is placed along the optical axis. The drift tubes, will provide the potential to trap the ions in the axial direction. To emit the electron beam, the HC-EBITs use one of the electron guns

designed at the Max Planck Institute for Nuclear Physics in Heidelberg, suitable for the job. The choice is either an on-axis or an off-axis electron gun, which has the advantage of leaving the optical axis free. Since for the purpose of spectroscopy with the calorimeter a free optical path is not needed, the *on-axis electron gun*, which is capable of a higher emission current due to its simpler design, was used. The collector, where the electron beam is dumped, can also be used for HCI extraction if attached to a beamline. The main CF cubic vacuum chamber is surrounded by soft iron pieces, which reinforces the magnetic field produced by stacks of *neodymium magnets* placed inside the *magnet enclosure*. The central vacuum chamber has 4 accessible ports. One of those ports is used by an injection system, while another is used for pumping. The other 2 free ports can be used to attach other measuring instruments, like detectors or spectrometers. In the constructed EBIT a beryllium window is installed at the top port where it will be pointing directly to a calorimeter.

### 3.1.2 The unique setup

The EBIT which has been constructed in the framework of this work is intended for high precision measurements with a microcalorimeter. In order for the EBIT to be able to fit below the already existing microcalorimeter setup, clear dimensional constraints were given. Figure 3.2 shows the dimensions of the calorimeter setup from which the constraints were taken.

These constraints have been satisfactorily fulfilled, culminating in one of the most compact HC-EBITs to date.

Figure 3.3 shows a picture of the final arrangement. The EBIT is mounted onto a frame consisting of aluminium construction profiles. Thanks to the locking wheels, the EBIT can be moved around easily. Once in place, the height can be adjusted with four levelling feet to the desired height shown in figure 3.2.

Most of the vacuum system is attached to one of the sides of the frame structure. To the opposite side, the injection system is attached. This keeps the EBIT compact and as shallow as possible while making movement and transportation of the EBIT easier.

Mostly everything is attached securely to the main frame structure, with the exception of both the scroll-pump and the water-cooler, which can fit below the EBIT, and the control rack.

The control rack shown in figure 3.1.2 is an additional frame made out of the same type of aluminium construction profiles. It contains all the necessary equipment to operate and monitor the EBIT. The following sections describe the individual components of the EBIT in more detail.

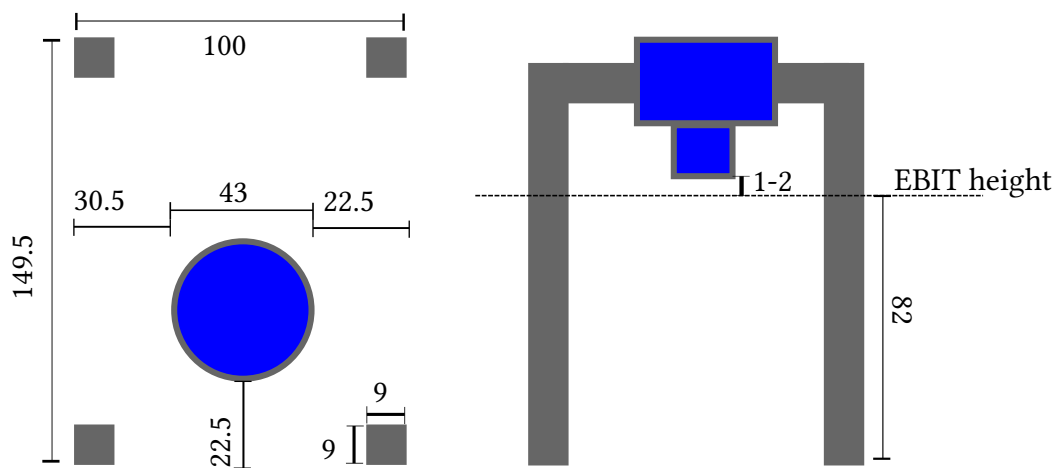


Figure 3.2: A diagram of the maXs-30 metallic magnetic calorimeter setup with the relevant dimensional measurements that represent the spatial constrains for the construction of the EBIT. The calorimeter is represented in blue and in grey the structure that lifts it from the ground. On the left the bird's-eye view that make for the length and width constrains in the construction. On the right a front view that makes for the height constrains. All dimensions are given in centimetres.

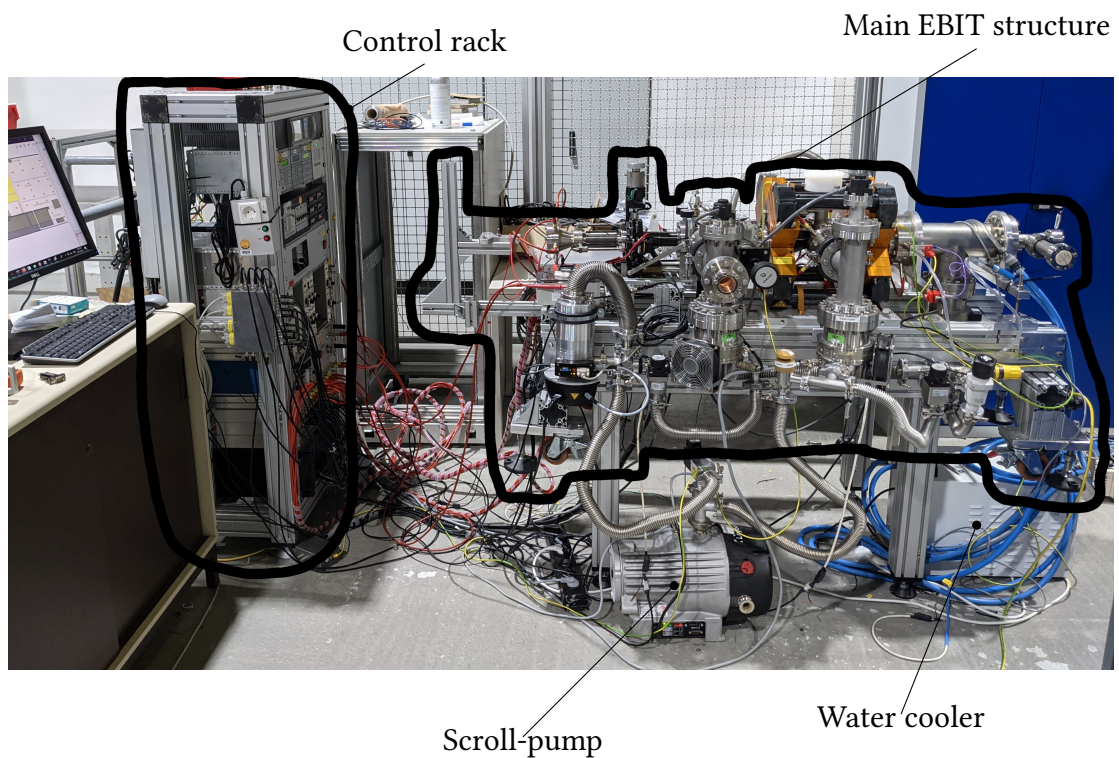


Figure 3.3: A picture of the laboratory showing the arrangement of the EBIT. The main EBIT structure has to fit below the microcalorimeter setup. The control rack can be placed besides the microcalorimeter setup since it is only connected to the EBIT through the necessary cables. The water cooler and scroll-pump have to be moved alongside the main structure and can fit either beneath or besides the EBIT.



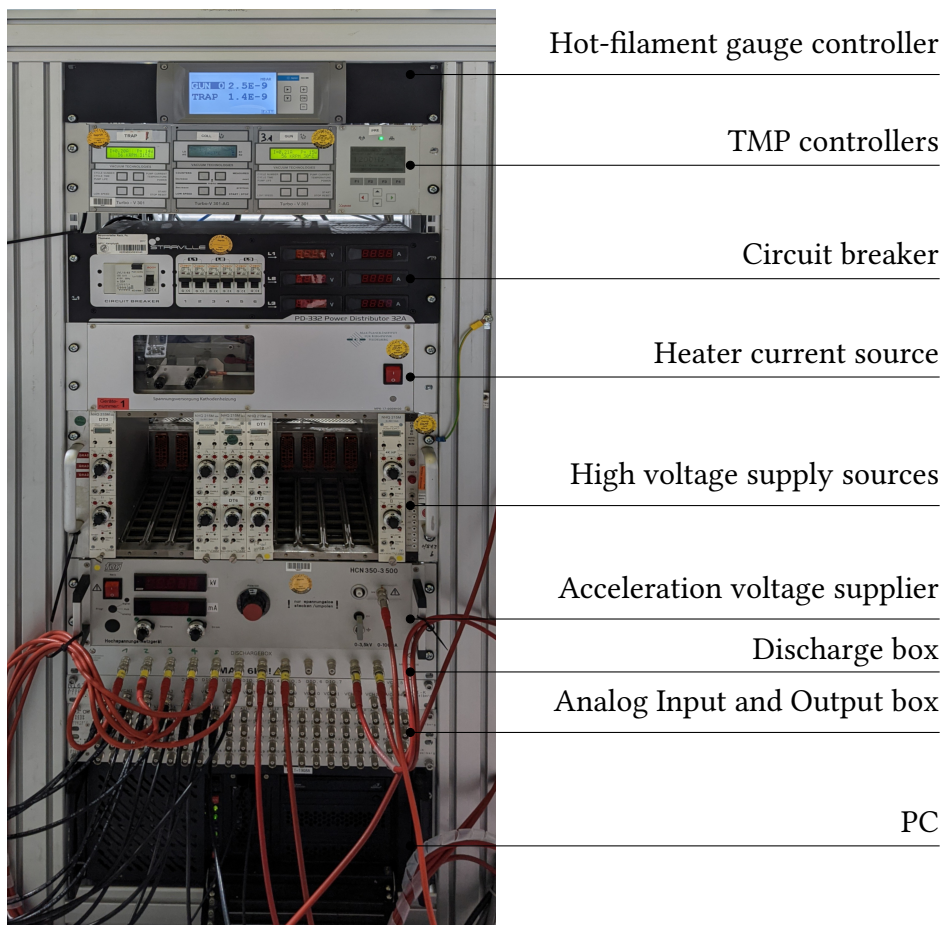


Figure 3.4: The control-rack of the EBIT. From top to bottom: The first controller controls the hot-filament ionization gauges and serves as a readout for the vacuum level. Below it the controller for the 4 turbomolecular pumps. The circuit breaker makes managing the power input to the equipment easier. Below it the source for the heater current applied through the cathode. The high voltage supply sources provide the voltage applied to the drift tubes, the focus and anode of the electron gun and the extraction electrodes of the collector. The voltage supplier below them supplies the acceleration voltage between the cathode and the anode of the electron gun. The discharge box is an extra security that provides a safe way for the high voltage power suppliers to get discharged. The analog Input and Output box makes the control of equipment connected to it and the PC below it possible.

## 3.2 The magnetic structure

In order to keep the EBIT a compact size, instead of using large superconducting coils that have to be cryogenically cooled, like e.g. the FLASH-EBIT [3], all of the HD-compact EBITs use 72 permanent neodymium magnets to generate the magnetic field. The magnets are arranged symmetrically in 4 alumina enclosures around the optical axis. Covering the outer part of the enclosure, 4 ferromagnetic rod handles are placed in order to increase the overall magnetic force, as well as guiding the magnetic structure.

### 3.2.1 Assembling the magnetic structure

Handling the magnets can be dangerous. They have to be put into the magnet enclosure one by one, to avoid them getting attracted by each other. During the operation wearing protective gloves is recommended to prevent damage caused by an uncontrolled collision while the magnet is held. To get the cylindrical magnets into the enclosure they are first inserted into a special tool designed specifically for this purpose. It consists of a long and hollow brass cylinder with a diameter slightly larger than the diameter permanent magnets. A piston system inside the brass cylinder drives a magnetic plate through the brass cylinder. The individual magnets can be placed into the magnetic plate and then be driven far inside the brass cylinder. The brass cylinder can be then inserted into the aperture of the magnet enclosure and the magnet can be slowly driven towards the enclosure. When other magnets are already inside the enclosure the tight fit and the eddy currents will prevent the magnet from colliding against each other.

### 3.2.2 Measuring the magnetic structure

After the magnetic structure was assembled, some measurements were taken to characterise the magnetic field. Of special interest here is the magnetic field strength and structure at the trap centre. It is not a given that the magnetic structure will be fitting, in the case of the XUV-EBIT, the magnetic field was not strong enough and additional permanent magnets had to be added to increase the magnetic field strength.

The results of the measurements assure the homogeneity of the magnetic structure at the trap center and found the the field strength maximum at 860 mT.

For the measurements a fitting axial Tesla meter was mounted to the XYZ-manipulator, used later to control the positioning of the electron-gun. The XYZ-manipulator allow for controlled movement in 3 dimensions with high precision. The XYZ-manipulator was then used to move the mounted tesla meter inside of the main cubic vacuum chamber and find the maximum magnetic field strength. The maximum magnetic strength lays on the middle of the cubic vacuum chamber (along the optical axis) as expected. With a different handheld tesla meter, the strength around and inside the magnetic

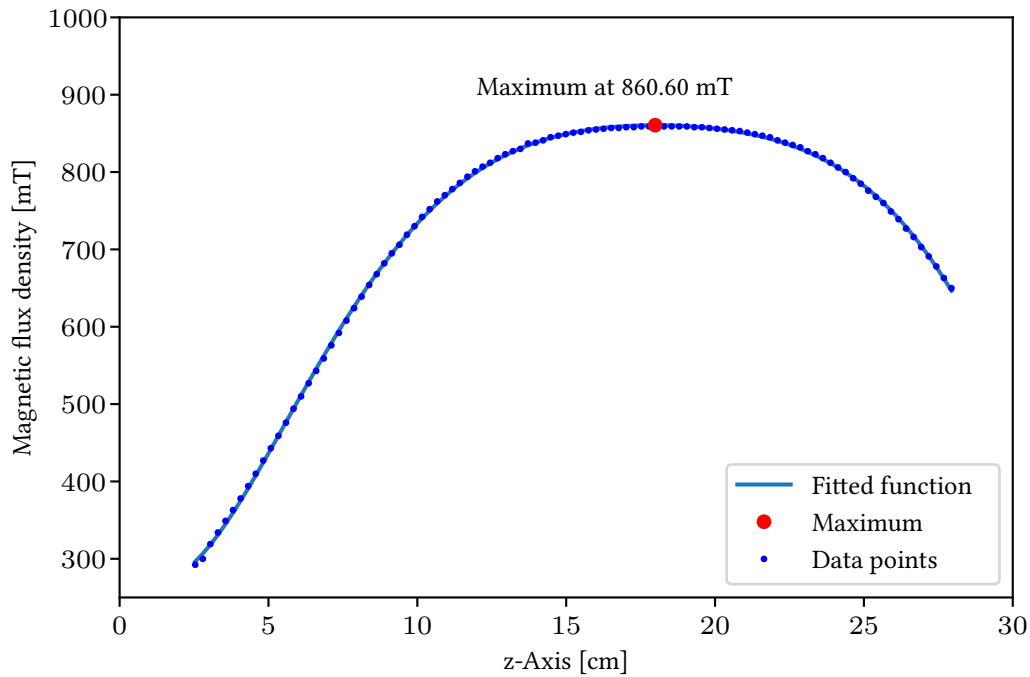


Figure 3.5: The magnetic force along the z-Axis.

structure was also measured, to assure no anomalies. Once the maximum was found, some measurements with the axial tesla meter mounted to the XYZ-manipulator were taken along the optical axis. Figure 3.5 shows one of such measurements in a region of 30 cm along the z-Axis. To investigate the behaviour of the magnetic field a 6th order polynomial was fitted to the datapoints. From the fitted function a maximum of 860.6 mT was calculated. The results show a similar structure and magnetic strength maximum to those of other HC-EBITs.

### 3.3 The electron gun

The electron gun emits the electrons that form the electron beam. At its simplest form an electron gun consists only of a cathode and an anode. The cathode is heated with a high current and between the cathode and the anode, a high acceleration voltage is applied, as depicted in figure 3.6.

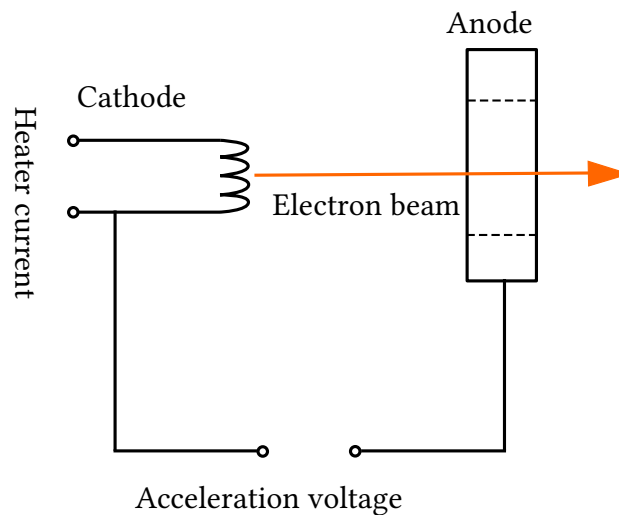


Figure 3.6: Diagram illustrating the concept of an electron gun.

Figure 3.6 is only a simplified concept and would not make for a very effective electron gun. Much more thought goes into designing a functional and efficient electron gun. The on-axis electron gun designed at the Max Planck Institute for Nuclear Physics is based on the design factors explained on [15].

The electrons forming the beam of the constructed EBIT are emitted from the cathode via thermal emission. Heating the cathode to temperatures in the magnitude of 1300 K provides the electrons with enough thermal energy as to overcome the work function of the cathode. The work function is dependent on the material and properties of the cathode. The barium-impregnated tungsten dispenser cathode used in the construction of this EBIT has a work function of around 2 eV [10]. The negative voltage applied to the anode, provides the big potential difference that repel and accelerate the electrons. A typical potential applied to the anode is in the order of 3 kV. A picture and render of the computer assisted design model is shown in figure 3.7. Between cathode and anode an extra electrode at a small negative potential compared to the anode potential focuses the electrons, hence the name focus electrode.

In the final assembly of the electron-gun the cathode filament has to be put in place. Since the filament is very sensible, to reduce air exposure time, the assembly process

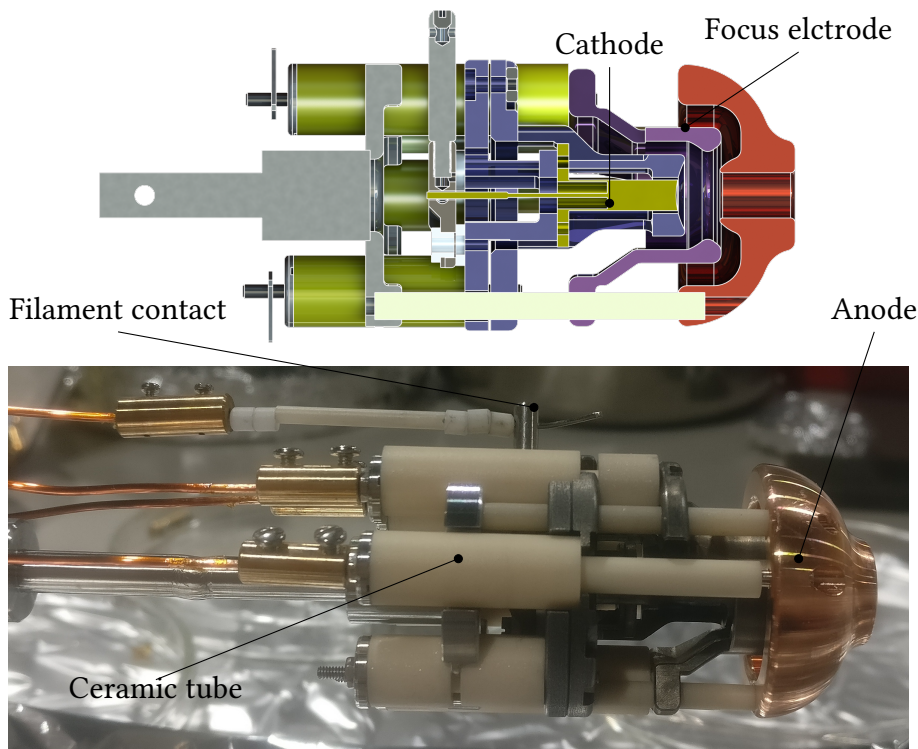


Figure 3.7: At the top a rendered cross section of the CAD model of the on-axis electron-gun of the HC-EBITs. At the bottom a picture of the electron gun used in the EBIT is shown.

should be done as quick as possible. For this reason one should rehearse the assembling, without the filament, multiple times.

Because the ceramic tubes and rods seen in fig 3.7 are prone to breakage, if using the same on-axis gun design it is best to file the ends of the rods carefully with a diamond file to make the electron gun assembly easier. To reduce air exposure even further, the final assembly was done under a nitrogen atmosphere.

Once the electron gun is inside the vacuum chamber, it has to rest close to DT1. The gun's position is adjustable using the XYZ-manipulator described in the previous section. To hold the electron gun in its place inside the vacuum chamber a simple steel rod was designed that can be mounted to the XYZ-manipulator.

### Designing a rudimentary Z-axis manipulator

A straight propagation of the electron beam through the optical axis towards the collector can only be achieved by tuning the position of the electron gun very precisely.

Small variations, in the mm range, in the position of the electron gun can have a huge impact in the transmission parameter. In other words, positioning the electron gun in such a way that the electron beam gets dumped inside the collector instead of hitting the drift tubes, is not an easy task. To allow this fine tuning of its position, the electron gun was mounted to an XYZ-manipulator.

For reasons that will become more clear in the section describing the vacuum system the XYZ-manipulator available at the time did not allow for enough movement in the Z-direction. For this reason a low-cost rudimentary Z-manipulator was designed using readily available parts. This manipulator seen in fig 3.8 , while keeping the overall design compact, allows for enough movement in the z direction and provides a stable locking mechanism for the electron-gun to rest safely in both its compacted and extended position. The manipulator consists of a vacuum bellow that is kept on a compressed position by three threaded rods with three nuts each. When the electron gun has to be moved above the XYZ-manipulator's capacity, the nuts on the threaded rods of the rudimentary manipulator can be unscrewed unlocking it from its compressed position. It can then be extended along the z direction.

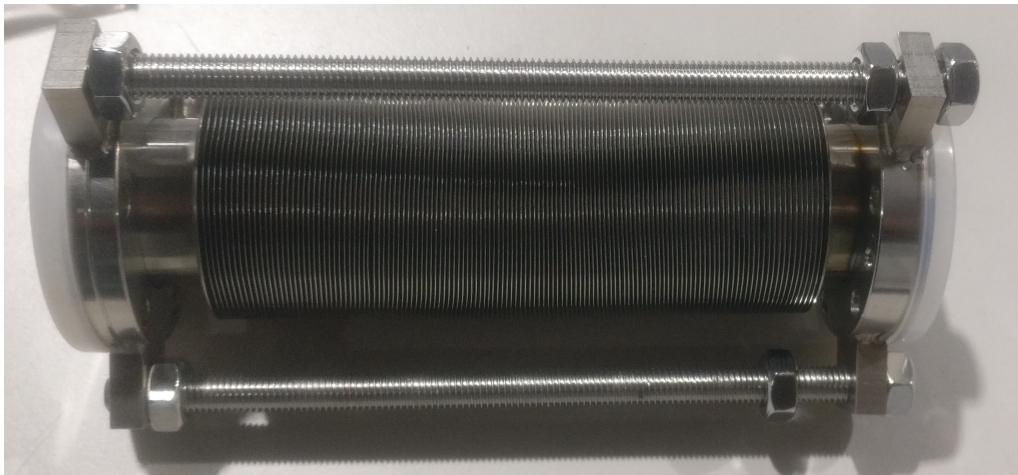


Figure 3.8: The designed rudimentary manipulator. A vacuum bellow is held in its compressed position. By unscrewing the nuts additional movement along the z-Axis is permitted.

### 3.4 The drift tubes

A drifttube (DT) is a cylindrical electrode that is held at a constant potential. Located inside the main cubic chamber along the optical axis 6 DTs guide the electron beam towards the collector, while providing the potential for trapping the ions in the axial direction. Fig 3.9 shows a photograph of the drift tube-assembly used in the construction of the EBIT. The assembly consists of 6 individual drift tubes made out of titanium alloy clamped together with 2 stainless-steel holders. 7 alumina-ceramic rods determine the distance between each drift tube while providing structural integrity to the assembly and keeping the drift tubes insulated from one another.

Of special interest are DT3, DT4 and DT5. DT4 is the trap center, placed at the middle of the main cubic chamber, where the magnetic flux density is at its maximum. In order to shape the trap potential DT3 and DT5 are held at the same potential, higher than the DT4 potential. The potential difference between DT3 and DT5 with respect to DT4 determine the potential depth.

To release the ions from the trap a voltage higher than the voltage applied to DT3 and DT5 can be applied.

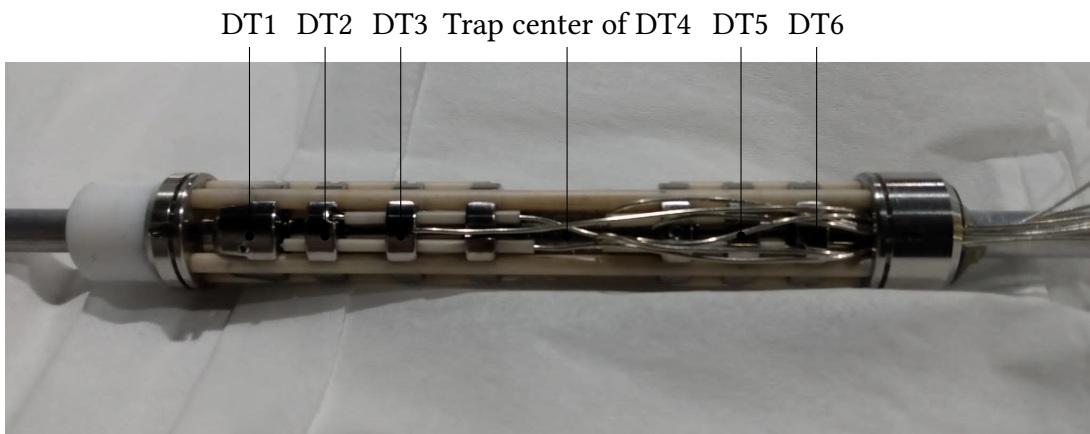


Figure 3.9: A picture of the drift tubes after the assembly. The drift tubes are clamped together by two metallic holders to make the installation inside the main cubic vacuum chamber possible. All the wires run through one of the holders so that they don't spread apart during the installation.

The wired drift tube assembly was positioned inside the main cubic structure. Each DT is wired independently to a high vacuum feed-through, which is then connected to voltage power supply. Ceramic beads were used as insulation between the cables. After the assembly each drift tube was tested and conditioned with voltages over 5000 V.

This values have been found by an iterative trial and error process as follows:

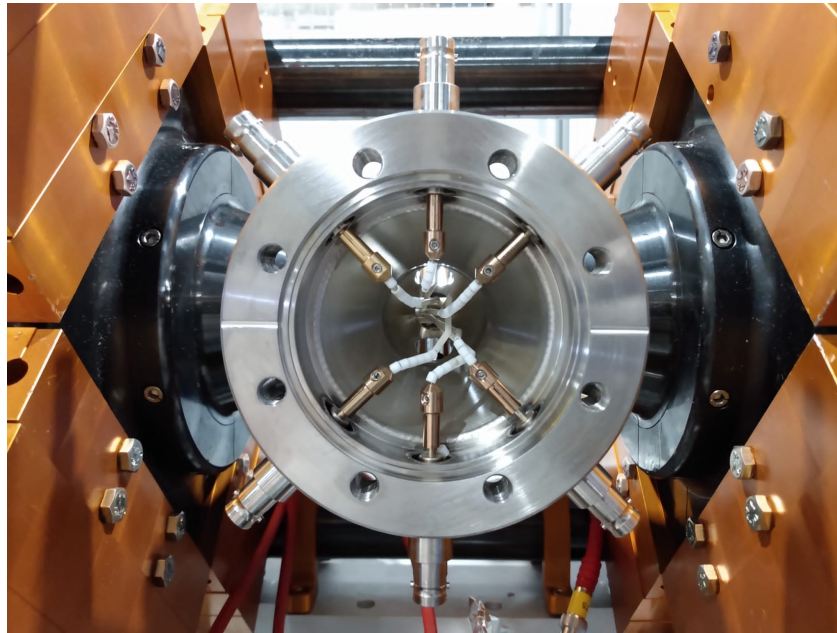


Figure 3.10: A picture of the wiring process of the drift tube assembly. The drift tubes were inserted into the main cubic vacuum chamber and then each drift tube was connected to a high vacuum feed-through. The cables were insulated with ceramic beads.

1. Getting the electron gun in a centred position. This can be done by eye. By looking through the window installed in front of the electron gun one can see the glowing cathode when the electron gun is centred.
2. Fine tuning the position of the electron gun.
3. Adjusting anode and focus electrode.
4. Adjusting all DT voltages.
5. Repeating the steps 2-5 until the transmission can not be optimised further.



DT number	Applied voltage [V]
1	1155
2	2699
3	574
4	1011
5	1027
6	-1826

Table 3.1: The fine-tuned values found in order to optimise transmission of the electron beam. This values were found at a cathode voltage of  $-3.032$  kV achieved a transmission of about 96%. The comparison to other HC-EBITs reveals an unusual behaviour. DT6 is usually grounded but in this case it had to be held at a high negative voltage.

### 3.5 The collector

The drift tubes guide the electron beam towards the collector. Because the magnetic field strength at the collector is much lower than at the trap center, the beam expands hitting the electrode wall. The collector electrode is hollow and made out of oxygen-free copper, for high thermal conductivity. The collector is additionally water cooled.

Two extraction electrodes are installed behind the electrode. They prevent the electron beam going through the collector and they can be used to extract the HCl into a beamline, hence the name extraction electrode.

In order for the electron beam to be successfully stopped, the first extraction electrode has to be biased with a potential more negative than the cathode.

The high current present at the collector can represent a deadly hazard, it is very important to make sure the whole EBIT and specially the collector is properly grounded.

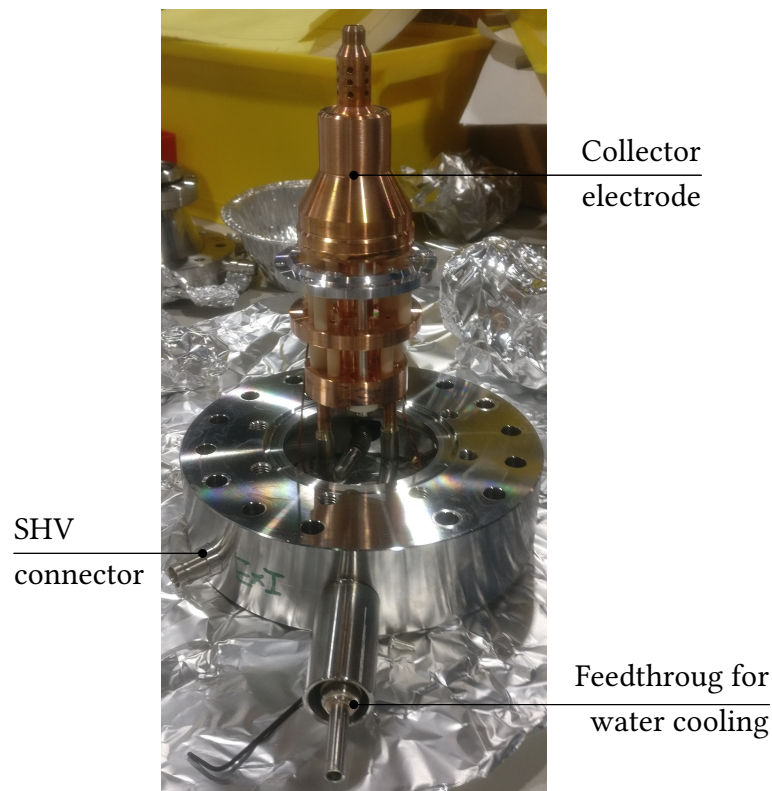


Figure 3.11: A picture of the collector used in the construction of the EBIT.

Of special interest is the *transmission* parameter  $T$ , which is the quotient between the *emission current*  $I_b$  and the *collector current*  $I_{coll}$ :

$$T = \frac{I_{coll}}{I_b} \quad . \quad (3.1)$$

A good transmission is considered to be above 95%. This parameter is very dependent on the positioning of the electron gun, the voltages applied to the drift tubes and the vacuum inside the vacuum chambers. A good transmission also hinders an excess current to reach the high voltage suppliers, potentially damaging them.

### 3.6 The vacuum system

The vacuum system is an essential part of an EBIT, it is crucial for the production of HCIs. Firstly the emission and transmission current is dependent on the vacuum level at the cathode. Furthermore a good vacuum inside the trap will prevent residual gas from recombining with the HCIs.

The EBIT makes use of 4 TMPs and a scroll pump in order to create UHV at around  $10^{-9}$  mbar inside the main chambers of the EBIT.

A  $300 \text{ l s}^{-1}$  TMP is connected to the electron-gun-, another at the ion-trap-, and a third one at the collector chamber. The output of each of the three TMPs is connected to a smaller  $70 \text{ l s}^{-1}$  TMP. This fourth's TMP output is connected to a scroll-pump. The setup is depicted in figure 3.12, the chambers and their connected surroundings, where the electron gun, the trap center and collector are inside, are labeled GUN, TRAP and COLL respectively.

All the chambers and the 3 TMPs connected to them are connected through standard CF components. The smaller TMP is connected to the output of the other TMPs and the input of the scroll pump through a series of ISO-KF components.

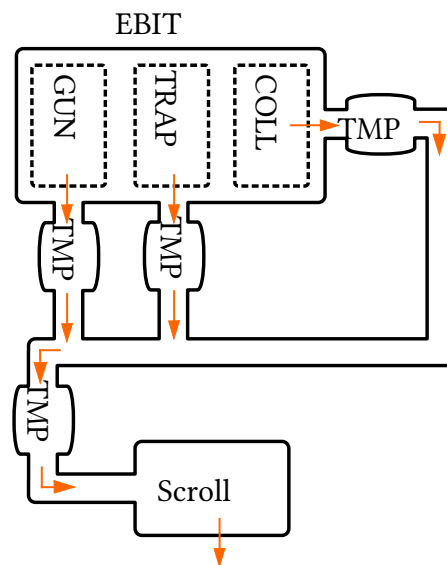


Figure 3.12: Schematic view of the simplified vacuum setup. The vacuum chamber of the electron-gun, ion trap and collector are labeled GUN, TRAP and COLL respectively. The turbomolecular pumps are labeled TMP and the scroll-pump as Scroll. The particle flow generated by the vacuum system is represented by the orange arrows.

To generate the vacuum first the scroll pump is turned on. After about 10 min. a clear

sound reduction from the scroll pump indicates the absence of major leakages and a vacuum around 1 mbar inside the EBIT can be assumed. After the scroll-pump, the TMP connected to the scroll-pump input can be turned on, followed by the remaining TMPs. After around 15 minutes the TMPs should have become quieter and be operating at around . At this point the three hot-filament gauges located at the input of the bigger TMPs can be turned on. The hot-filament gauges used for readout of the vacuum level can only operate between high- and ultra-high-vacuum and will burn out below the  $10^{-3}$  mbar level.

To prevent damage to the cathode, it has to be kept under vacuum, since the cathode's filament oxides, which shortens its lifetime significantly.

Therefore the vacuum system was designed with the capability of isolating the vacuum in the electron-gun chamber. With the electron-gun positioned in the electron-gun chamber and the vacuum in the gun area fully isolated, the remaining chambers can be opened up to atmospheric pressure, without damaging the cathode of the electron-gun. This eases issue tracking and repair-ability. It also makes for a more flexible EBIT design, since an easier access in the collector and trap area could allow for a re-purposing of the machine. For example, a different detector, injection system or a complete beamline could be attached to the EBIT.

Making the vacuum separation possible, a linear valve was installed between the electron-gun and the ion-trap chamber and additional valves at the output of the gun-, trap- and collector-pumps. The final vacuum system with the location of the aforementioned valves in blue is represented in figure 3.13. Closing this valves complete the vacuum isolation and make it possible to open the trap- and coll- chamber to atmospheric pressure, with there vacuum system still fully functioning in the electron-gun area.

If for some reason an exchange of the smaller TMP is necessary, the valve at the output of the pump connected to the electron-gun chamber (represented in light blue in figure 3.13) can be closed. Any work executed at this point has to be done quickly since the working TMP, has a small available volume for vacuum deposition and won't be able to maintain a good enough vacuum for more than a couple of hours.

A caveat presents itself when reinstating the vacuum in the trap and collector chambers. The smaller TMP should not be used at atmospheric level. Ideally a medium vacuum should be present before starting the TMP.

By installing a bypass system, the scroll-pump can be used to get the trap and collector chambers to the required vacuum level, before operating the smaller TMP and the TMPs located at the trap- and collector-chamber.

The valve between the scroll and the small TMPs output is a self locking valve, that will close itself in case of a power outage. In such a scenario the preserved vacuum would be good enough to not cause damage to the electrons gun cathode for several days.

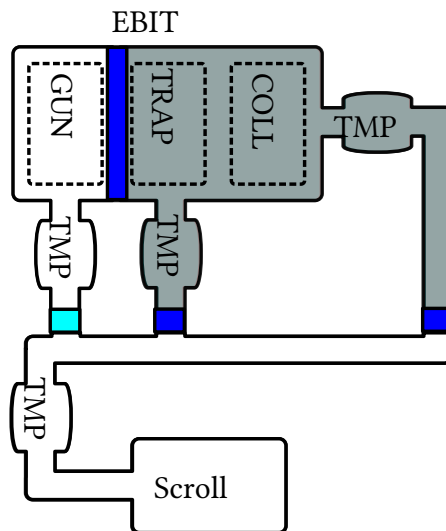


Figure 3.13: Diagram pointing the location of the valves that make the vacuum-separation possible. When the dark blue valves are closed and the light blue valve open the vacuum in the grey region is isolated from the vacuum in the rest of the EBIT.

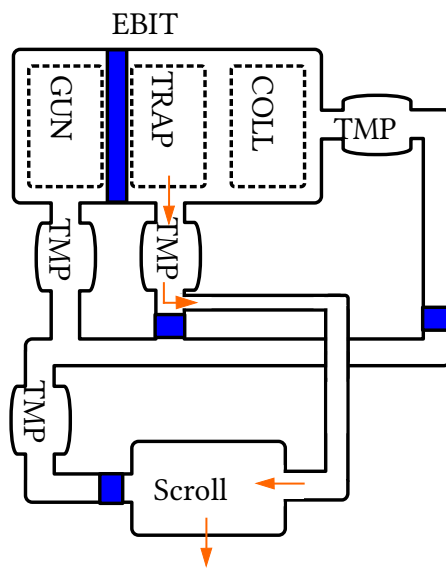


Figure 3.14: Diagram of the bypass system. The closed valves are represented in blue. The vacuum in GUN is isolated from the vacuum at TRAP and COLL. The particle flow from TRAP and COLL through the bypass system is represented by the orange arrows.

The reason why the additional Z-axis manipulator presented in the electron gun section was designed can be understood from figure 3.13. The electron gun while in operation rests at a distance from about a few centimetres to a few millimetres near of DT1. This means that the electron gun and the metallic rod holding it in place extend from the electron gun vacuum chamber into the ion trap vacuum chamber. One of the valves that make the vacuum separation possible has to be installed between this two chambers. Therefore whenever a vacuum separation due to any reason is needed the electron gun has to be moved further into the electron gun chamber than what is possible without the additional Z-axis manipulator.

### 3.7 Injection system

The injection system, a diagram in fig 3.15 consists of a gas cylinder connected to a pressure reducing valve and needle valve. The pressure reducer reduces the gas pressure inside the gas cylinder from about 10 bar to 2 bar .

The needle valve, that allows for a very thin stream of gas, is connected to the central CF cubic vacuum chamber via a standard DN 40 CF full nipple and to the gas cylinder via a swage metal capillary. On the inside of the DN 40 CF full nipple another metal capillary guides the gas to the inside of the central CF cubic vacuum chamber into the ion trap. When connecting the needle valve to the full nipple and the full nipple to the CF-cube it is important to make sure that the metal capillary points toward the drift tube. Once fully assembled the valve can be opened slightly, the pressure difference between the EBIT and the gas cylinder will let some of the gas into the trap. Figure 3.16 shows a photograph of the injection system with an argon gas cylinder. If any other gas is to be injected into the ion trap it is to be made sure that there is no remaining argon. For this, inverting the trap potential and changing the gas cylinder is not enough. One has to make sure, that there is no argon remaining in the injection system itself. The purpose of the valve installed between the gas cylinder and the needle valve is to serve as an extension for a diaphragm pump. When the argon cylinder is exchanged for another gas cylinder, the valve is opened and the connected diaphragm pump will pump out the residual gas.

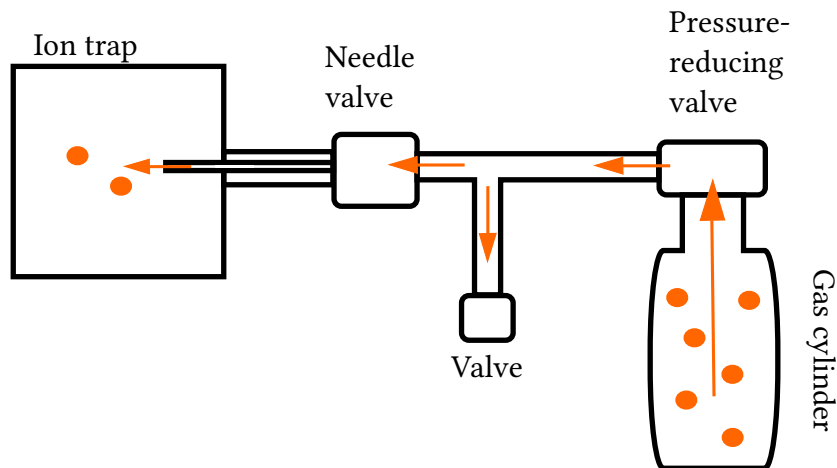


Figure 3.15: Diagram showing the most important components of the injection system. Particle flow with an opened needle valve and pressure reducing valve is represented by the orange arrows.



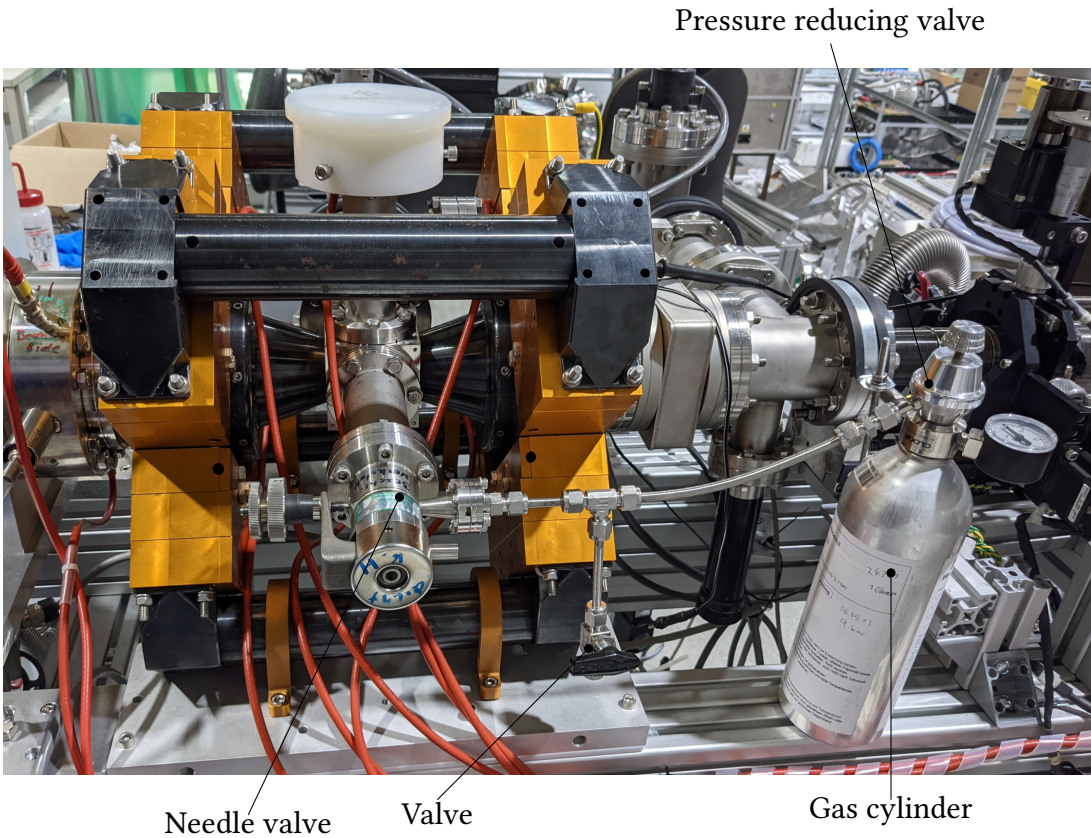


Figure 3.16: The injection system of the EBIT with the more important components labelled. The injection system is currently connected to an argon gas cylinder.



## 4 A first spectrum

For the purpose of testing the capabilities of the EBIT to trap and ionize ions, a proof-of-principle experiment was conducted. A Silicon Drift Detector was mounted on top of the beryllium window of the EBIT. Using the installed injection system, a constant flow of neutral Argon was introduced into the interaction-zone of the EBIT. By setting the electron-beam energy above the threshold of direct excitation, the X-ray spectrum was observed. Various emission lines have been detected, that were expected to be attributed to the interaction of the electron beam with elements, spluttered from the electrode-material and to the argon gas. To allow proper identification, the detector has been calibrated using a radioactive Americium source.

Initially, the detector, that already incorporates a beryllium window, was attached directly to the cubic CF structure. However the detector had a leak that made the vacuum at the trap chamber fall under the  $10^{-6}$  mbar level.

Since this was the only suitable detector available at the time a system had to be designed quickly to circumvent the leakage problem.

Therefore a beryllium window was installed at the top port of the main cubic vacuum chamber of the EBIT and the detector was placed on top of it, outside the vacuum. This means that there were 2 beryllium windows and a few millimetres of air in between the detector and the ions.

### 4.1 Calibration

Americium-241 is a radioactive isotope of americium. Apart from being used in smoke detectors, the americium isotope is a great source for energy calibration. It decays mainly via alpha decay with a gamma ray byproduct. It leaves a characteristic spectrum in the X-ray range behind.

Therefore if an americium spectrum is given, where the energy of some characteristic peaks are already known, one can hopefully identify the same peaks in an americium spectrum taken by the detector to be calibrated.

Figure 4.1 shows the taken americium-241 spectrum (in blue). A region of interest (in orange) was chosen to which a function was then fitted (green). The chosen function is a summation of 14 gaussian functions:

$$\sum_{i=1}^{14} \frac{A_i}{\sqrt{2\pi}\sigma_i} \exp\left(-\frac{(x - \mu_i)^2}{(2\sigma_i)^2}\right) . \quad (4.1)$$

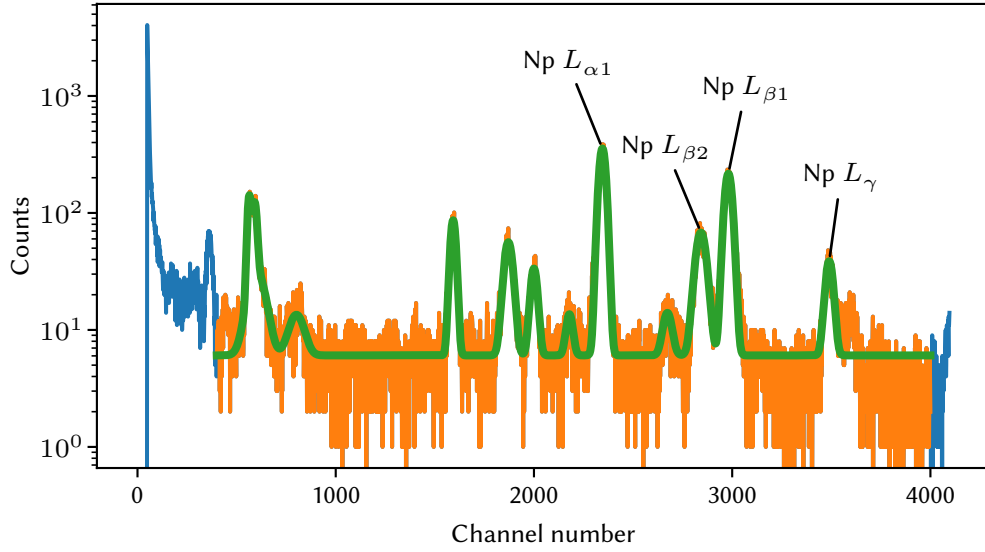


Figure 4.1: The recorded Americium-241 spectrum (blue) was fitted over a region of interest (orange).

From the parameters obtained from the fit, the position of the channel number for each of the identified peaks was matched with the corresponding energy.

Peak	Channel number	Corresponding energy [keV]
Np $L_{\alpha 1}$	$2345.245 \pm 0.068$	13.9441
Np $L_{\beta 2}$	$2842.36 \pm 0.47$	16.84
Np $L_{\beta 1}$	$2980.82 \pm 0.19$	17.7502
Np $L_{\gamma}$	$3489.484 \pm 0.76$	20.77

Table 4.1: Peak identification Americium

By plotting the detector's channel number against the correspondend energy for each peak Transformation such that

$$a \cdot (\text{Cannel number}) + m = \text{Energy} \quad (4.2)$$

with parameters  $a = 0.005\,974 \pm 0.000\,057$  and  $m = -0.087 \pm -0.166$

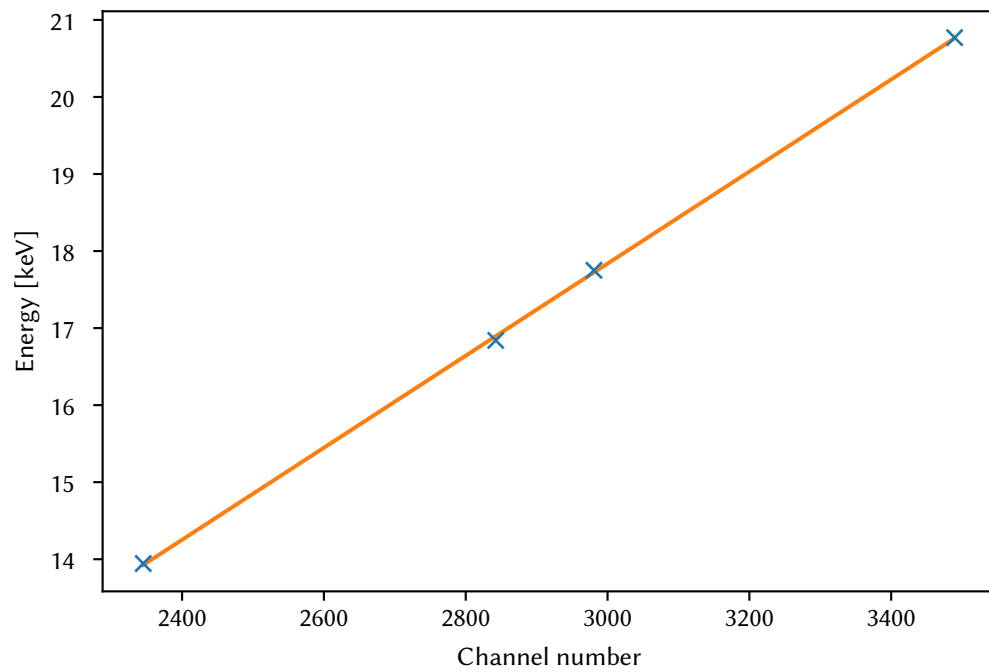


Figure 4.2: Four X-ray lines in the americium spectrum were successfully identified and plotted over their respective energy (blue). The linear calibration function is depicted in orange.

## 4.2 The argon spectrum

As a next step the Silicon Drift Detector was mounted on top of the trap center of the EBIT. Using the injection system, a constant flow of argon gas was injected into the trap. The electron beam energy was set to approximately 4keV to ensure direct excitation of Argon between  $n=1$  and  $n=2$ . The resulting spectrum, shown figure 4.3, was taken over a time-span of few days due to the low event rates caused by the small solid angle between the detector and the ions, the two beryllium windows and few millilitres of air in between. 11 lines have been determined from the obtained spectrum by modelling the experimental data with a summation over gaussian profiles. With the use of above calibration function the corresponding energy values were determined (see table 4.2).

It was expected that line 4 could be attributed to a signal produced by direct excitation of argon, and that the lines 5.57 keV and 6.38 keV, the highest energetic lines, due to radiative recombination into  $n=2$  and  $n=3$  and the remaining lines due to excitation of the spluttered elements of of the drift-tube material. However the lines could not be matched to known argon lines or to lines due to typical elements found inside the EBIT. This could indicate that the calibration function is not suitable. A reason for this could be that not enough peaks were identified in the americium spectrum to perform a proper calibration. More peaks should be identified in the future. Since the identification of americium lines in the lower energetic range was difficult, the resulting calibration function does not overlap with the

Channel number	Corresponding energy [keV ]
179.12	0.98
244.96	1.38
423.52	2.44
478.04	2.77
524.52	3.05
607.70	3.54
695.90	4.07
778.96	4.57
842.79	4.95
947.24	5.57
1083.04	6.38

Table 4.2: The peak position obtained from the fit parameters in channels and the corresponding energy

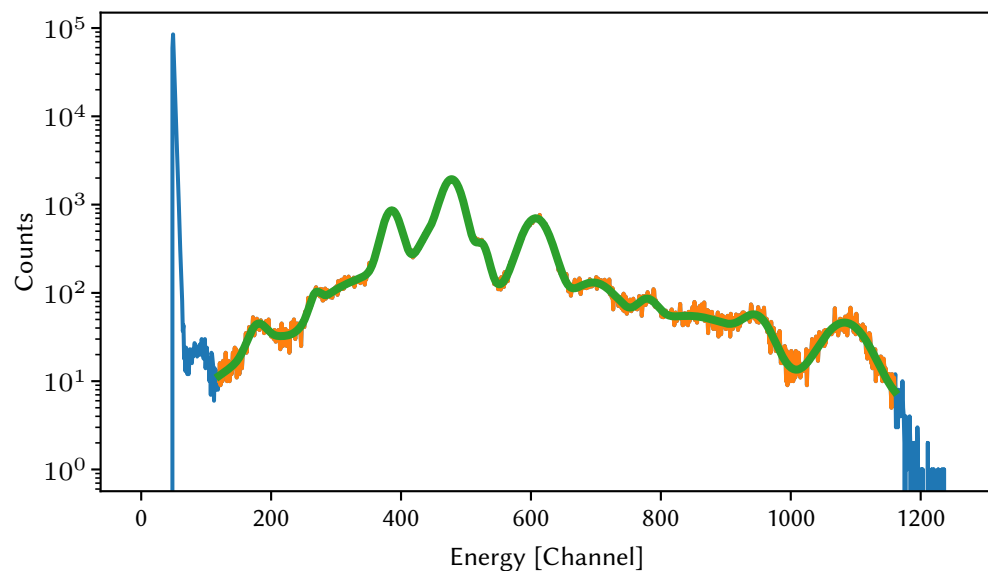


Figure 4.3: The argon spectrum (blue) was fitted (green) over a region of interest (orange).





## 5 Summary and outlook

In this work a new HC-EBIT was constructed while implementing the design decisions necessary to accommodate a collaboration with an already existing maXs-30 metallic magnetic calorimeter. In first tests, the EBIT produced emission currents up to 6 mA with transmissions over 95%.

Originally the idea was to build the EBIT, transport it to the Kirchhoff-Institute for Physics at the Heidelberg University where the group led by Loredana Gastaldo keeps the metallic magnetic calorimeter and record high resolution measurements with it. Unexpected problems with the EBIT, still unresolved at the time of writing this thesis, force a postponement in the collaboration with the calorimeter.

At the time of finishing this thesis, two factors have been identified as the possible cause of the problems. The first one is a major fault in the building process involving the drift tube assembly. The hypothesis is that the drift tube was not positioned correctly and became loose during or after the insertion into the main cubic vacuum chamber. This hypothesis could explain the unusual high negative voltage that had to be applied to DT6 during the fine tuning of the transmission. A poorly centred DT6 could have caused a constant impact of the electron beam against it. This would explain that such a high negative potential had to be applied to DT6. In such a case DT6 would have to act similar to a focus electrode in order for the electron beam not to hit it and transmission to be good.

A loose drift tube assembly could explain the sudden losses of emission current that happened on several occasions. One possible explanation is that the loose drift tube could have caused voltage discharges that could have even damaged the cathode of the electron gun. When this hypothesis gained credence and other hypothesis were discarded, the vacuum chamber where the drift tubes are located was recently opened up to atmospheric pressure for closer inspection. The drift tube setup seemed to have been, in fact, loose but this is still mere speculation since it is impossible to tell if this was in fact the case before opening the vacuum chamber. The drift tubes are currently being reassembled.

Another hypothesis has to do with the rudimentary manipulator setup. It seems to be too rattly, especially while moving the electron gun. The setup, initially intended as temporary fix for the lack of an XYZ-manipulator of the appropriate length in the Z-direction, is far from ideal and should be exchanged in the future. If the vacuum chamber where the electron gun has to be opened, exposing the cathode to air, this

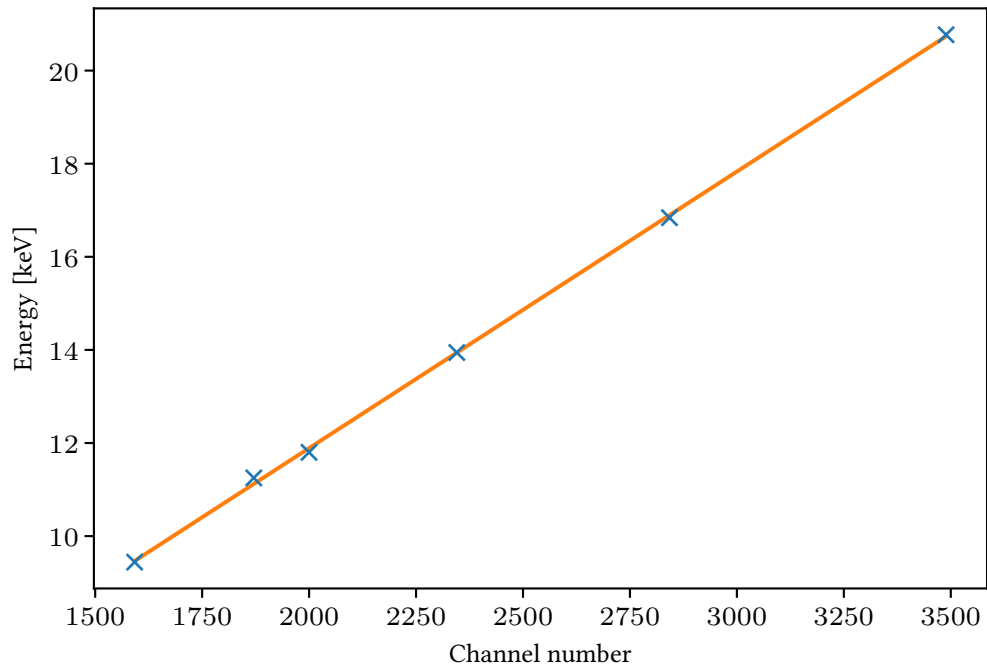


Figure 5.1: The new calibration function, left uninvestigated

would be a good opportunity for exchanging the manipulator.

The spectrum recorded while the EBIT was operational did not produce the expected results, since no lines were identified. The calibration function could be to blame here. Another calibration function with six lines instead of four has been obtained from the americium spectrum but it has not been further studied due to time constrains. The spectra should be further investigated in the future and/or other spectra should be recorded when the EBIT is operational again.

# Bibliography

- [1] European Space Agency. *XMM-Newton: Summary*. 2011. URL: <https://sci.esa.int/web/xmm-newton/-/31249-summary> (visited on 10/31/2021).
- [2] Stephen Clark. *Attitude control failures led to break-up of Japanese astronomy satellite*. 2016. URL: <https://spaceflightnow.com/2016/04/18/spinning-japanese-astronomy-satellite-may-be-beyond-saving/> (visited on 10/31/2021).
- [3] S W Epp et al. “X-ray laser spectroscopy of highly charged ions at FLASH”. In: 43.19 (Sept. 2010), p. 194008. DOI: [10.1088/0953-4075/43/19/194008](https://doi.org/10.1088/0953-4075/43/19/194008). URL: <https://doi.org/10.1088/0953-4075/43/19/194008>.
- [4] Taotao Fang and Claude R. Canizares. “Probing Cosmology with the X-Ray Forest”. In: 539.2 (Aug. 2000), pp. 532–539. DOI: [10.1086/309270](https://doi.org/10.1086/309270). arXiv: [astro-ph/0009305](https://arxiv.org/abs/astro-ph/0009305) [[astro-ph](https://arxiv.org/abs/astro-ph/0009305)].
- [5] A Fleischmann et al. “Metallic magnetic calorimeters (MMC): detectors for high-resolution X-ray spectroscopy”. In: *Nuclear Instruments and Methods in Physics Research Section A: Accelerators, Spectrometers, Detectors and Associated Equipment* 520.1 (2004). Proceedings of the 10th International Workshop on Low Temperature Detectors, pp. 27–31. ISSN: 0168-9002. DOI: <https://doi.org/10.1016/j.nima.2003.11.212>. URL: <https://www.sciencedirect.com/science/article/pii/S0168900203031103>.
- [6] J D Gillaspay. “Highly charged ions”. In: 34.19 (Sept. 2001), R93–R130. DOI: [10.1088/0953-4075/34/19/201](https://doi.org/10.1088/0953-4075/34/19/201). URL: <https://doi.org/10.1088/0953-4075/34/19/201>.
- [7] HEARSAC. *X-ray Imaging and Spectroscopy Mission (XRISM)*. 2021. URL: <https://heasarc.gsfc.nasa.gov/docs/xrism/> (visited on 11/02/2021).
- [8] Gabriel Herrmann. “Optical Theory of Thermal Velocity Effects in Cylindrical Electron Beams”. In: *Journal of Applied Physics* 29.2 (1958), pp. 127–136. DOI: [10.1063/1.1723053](https://doi.org/10.1063/1.1723053). eprint: <https://doi.org/10.1063/1.1723053>. URL: <https://doi.org/10.1063/1.1723053>.

- [9] Morton A Levine et al. “The Electron Beam Ion Trap: A New Instrument for Atomic Physics Measurements”. In: T22 (Jan. 1988), pp. 157–163. DOI: [10.1088/0031-8949/1988/t22/024](https://doi.org/10.1088/0031-8949/1988/t22/024). URL: <https://doi.org/10.1088/0031-8949/1988/t22/024>.
- [10] P. Micke et al. “The Heidelberg compact electron beam ion traps”. In: *Review of Scientific Instruments* 89.6 (2018), p. 063109. DOI: [10.1063/1.5026961](https://doi.org/10.1063/1.5026961). eprint: <https://doi.org/10.1063/1.5026961>. URL: <https://doi.org/10.1063/1.5026961>.
- [11] NASA/Harvard. *About Chandra*. 2015. URL: <https://chandra.harvard.edu/about/> (visited on 10/31/2021).
- [12] Gerry O’Sullivan et al. “Spectroscopy of highly charged ions for extreme ultraviolet lithography”. In: *Nuclear Instruments and Methods in Physics Research Section B: Beam Interactions with Materials and Atoms* 408 (2017). Proceedings of the 18th International Conference on the Physics of Highly Charged Ions (HCI-2016), Kielce, Poland, 11-16 September 2016, pp. 3–8. ISSN: 0168-583X. DOI: <https://doi.org/10.1016/j.nimb.2017.03.114>. URL: <https://www.sciencedirect.com/science/article/pii/S0168583X17303634>.
- [13] J. R. Rydberg Ph.D. “XXXIV. On the structure of the line-spectra of the chemical elements”. In: *The London, Edinburgh, and Dublin Philosophical Magazine and Journal of Science* 29.179 (1890), pp. 331–337. DOI: [10.1080/14786449008619945](https://doi.org/10.1080/14786449008619945). eprint: <https://doi.org/10.1080/14786449008619945>. URL: <https://doi.org/10.1080/14786449008619945>.
- [14] N. Bohr Dr. phil. “I. On the constitution of atoms and molecules”. In: *The London, Edinburgh, and Dublin Philosophical Magazine and Journal of Science* 26.151 (1913), pp. 1–25. DOI: [10.1080/14786441308634955](https://doi.org/10.1080/14786441308634955). eprint: <https://doi.org/10.1080/14786441308634955>. URL: <https://doi.org/10.1080/14786441308634955>.
- [15] J. R. Pierce. “Rectilinear Electron Flow in Beams”. In: *Journal of Applied Physics* 11.8 (1940), pp. 548–554. DOI: [10.1063/1.1712815](https://doi.org/10.1063/1.1712815). eprint: <https://doi.org/10.1063/1.1712815>. URL: <https://doi.org/10.1063/1.1712815>.
- [16] Eite Tiesinga et al. “CODATA recommended values of the fundamental physical constants: 2018”. In: *Rev. Mod. Phys.* 93 (2 June 2021), p. 025010. DOI: [10.1103/RevModPhys.93.025010](https://link.aps.org/doi/10.1103/RevModPhys.93.025010). URL: <https://link.aps.org/doi/10.1103/RevModPhys.93.025010>.

- [17] D. Unger et al. “High-resolution for IAXO: MMC-based X-ray detectors”. In: 16.06 (June 2021), P06006. doi: [10.1088/1748-0221/16/06/p06006](https://doi.org/10.1088/1748-0221/16/06/p06006). URL: <https://doi.org/10.1088/1748-0221/16/06/p06006>.

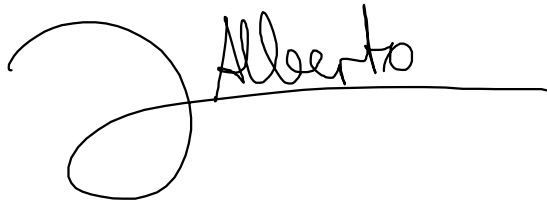
## **Acknowledgments**

The building of the EBIT was not a one person operation. Most of the work described in this thesis and most of the work that was left undescribed, like the fun and the pain of dealing with ultra high vacuum components and their million screws, was performed by Moto Togawa and myself. I hereby thank all he colleagues that lent a hand in the construction process and special thanks to Moto not only for all his work but also for his guidance and patience during the whole process.

# Erklärung

Ich versichere, dass ich diese Arbeit selbstständig verfasst und keine anderen als die angegebenen Quellen und Hilfsmittel benutzt habe.

Heidelberg, den 3.11.2021

A handwritten signature in black ink. The signature consists of a large, stylized initial 'A' followed by the name 'Alberto' written in a cursive script. A horizontal line extends from the end of the signature to the right.

Alberto Rodríguez Concepción